AIMS Bioengineering

AIMS Bioengineering, 12(3): 383–396.
DOI: 10.3934/bioeng.2025018
Received: 22 May 2025
Revised: 05 August 2025
Accepted: 11 August 2025
Published: 15 August 2025

https://www.aimspress.com/journal/Bioengineering

Research article

Energetics of pPF1 plasmid kinks

Ludmila V. Yakushevich[1,*] and Larisa A. Krasnobaeva[2]

[1] Institute of Cell Biophysics, Russian Academy of Sciences, 142290 Pushchino. Institutskaya str. 3, Moscow region, Russia
[2] Siberian State Medical University, 634050 Tomsk, Moscow tract 2, Russia

* **Correspondence:** Email: kind-@mail.ru; Tel: + 74967739252; Fax: +74967330509.

Abstract: Kinks are known in mathematics as special solutions of nonlinear partial differential equations (NLPDEs) and in biology as models of open states of DNA formed during replication, transcription, and denaturation. The characteristics of the formation and movement of kinks in various DNAs are currently being actively studied. However, the dynamic behavior of kinks formed and propagated in the recently synthesized plasmid pPF1 remains poorly understood, and the issue of kink energetics has not yet been considered. This paper considers the energetics of kinks moving in the potential field of the plasmid pPF1, the sequence of which consists of 5557 base pairs and includes the genes of fluorescent proteins *Egfp* and *mCherry*, separated by a small intermediate region, as well as the gene of resistance to kanamycin (*Kan*). The paper presents the calculations of the energy profiles of the plasmid potential field, as well as the time dependence of the energy, size, and propagation velocity of kinks along these strands. Considerable attention is paid to the study of the influence of DNA torque on the energy of kinks. It is shown that the form of the curves of dependence on time is completely determined by the magnitude of the torque. Thus, at torque values below threshold values, the energy curves have the form of damped oscillations; at torque values above the threshold values, the energy curves change smoothly. Estimates of these threshold values are provided.

Keywords: pPF1 plasmid; DNA open states; kink energy; kink size; kink velocity

1. Introduction

The DNA molecule has a unique double helix structure that provides stability and protection for

genetic information. However, this structure is not rigid. On the contrary, it has significant conformational mobility. Thus, the double helix can "open" or "denature" when one or more adjacent pairs of nucleotides break the complementary hydrogen bonds that hold them in the duplex. Opening of the DNA double strand provides enzymes with access to nitrogen bases; therefore, the open states are actively involved in specific DNA–protein interactions.

Many attempts have been made to create suitable models to explain the complex dynamics of DNA [1]. However, obtaining accurate model equations is quite a difficult task due to the numerous degrees of freedom and interactions [2]. Therefore, many researchers work with simplified models that take into account only one or two types of internal DNA motions. The most interesting models take into account the rotational oscillations of the nitrous bases. The first and simplest model of this type was proposed by Englander et al [3]. Kink-like solutions of Englander's model equation (or simply kinks) were interpreted as mathematical analogues of open states. The reason that motivated Englander et al. to focus exclusively on kink-type waves was that other types of solutions, such as breathers or pulses, have a rest energy, interpreted in biology as the energy of formation of DNA open states, greater than that of kinks.

Improved versions of Englander's model, which clarified and developed the concept of DNA kinks, were proposed by Yamosa [4], Takeno and Homma [5], Krumhansl [6], Fedyanin [7], and Yakushevich [8]. Recently, Grinevich et al. [9] proposed a new version of Englander's model, which demonstrates good correlation with experimental data. All the models mentioned above were used to study the features of kink formation and movement in various DNAs. However, kink dynamics in the recently synthesized plasmid pPF1 remain poorly understood, and the issue of kink energetics has not yet been considered.

In this paper, the energetics of kinks formed and moving in the plasmid pPF1 are investigated. We present the results of the energy profiles of the main and complementary strands of the pPF1 plasmid and the time dependence of the energy, size, and velocity of kinks propagating along the strands. The effect of DNA torque on kink energetics is also considered.

2. Materials and methods

The pPF1 plasmid was created by Masulis et al. in 2015 [10] as a tool for studying the functional properties of *Escherichia coli* DNA fragments containing promoter-like regions predicted by Shavkunov et al. [11]. Subsequently, the pPF1 plasmid was successfully applied by Masulis et al. [12] to study the relationship between the functional and dynamic properties of the *appY_red* and *appY_green* genetic constructions created by inserting *E. coli* fragments into the region of the pPF1 plasmid placed between the genes of red (*mCherry*) and green (*Egfp*) proteins.

The first steps in the study of the pPF1 plasmid itself, without any sequences integrated into it, were related to modeling its dynamic properties [13], including the formation and propagation of open states [14,15].

To model the pPF1 plasmid, the block method was used, in which the plasmid sequence was divided into several regions (or blocks): three functionally significant regions, namely the red protein gene *mCherry* [16] with coordinates 1134–1841, the green protein gene *Egfp* [17] with coordinates 333–1049, and the kanamycin resistance gene (*Kan*) [18] with coordinates 2569–3381, as well as the regions located between these three genes (Figure 1). The division made it possible to simplify mathematical calculations due to the use of a quasi-homogeneous method, according to

which the dynamic DNA parameters were averaged over each of the regions mentioned above.

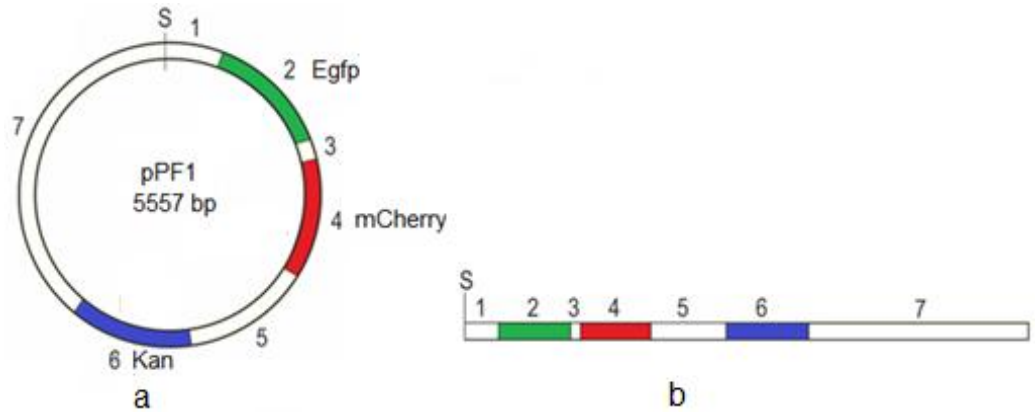

Figure 1. Circular (a) and linear (b) schemes of the pPF1 plasmid. S is the "cut" point. Numbers 1–7 indicate the region numbers.

In Figure 1, all 7 regions are shown. However, the pPF1 plasmid has a circular form. To take into account this factor, let us connect the ends of the linear sequence of the pPF1 plasmid and combine regions 1 and 7 into a single intermediate region. We will call this single region the (1+7) region. Thus, the total number of regions in the pPF1 plasmid becomes equal to 6 instead of 7.

To describe the dynamics and energetics of kinks in each of the regions, we use the model of Grinevich et al. [9]

$$\begin{aligned} & I_{\mathrm{n},1}\frac{d^2\varphi_{n,1}(t)}{dt^2} - K'_{n,1}\left[\varphi_{n+1,1}(t) - 2\varphi_{n,1}(t) + \varphi_{n-1,1}(t)\right] + \\ & + k_{n,1-2}R_{\mathrm{n},1}(R_{\mathrm{n},1} + R_{n,2})\,\sin\varphi_{n,1} - k_{n,1-2}R_{\mathrm{n},1}R_{\mathrm{n},2}\sin(\varphi_{n,1} - \varphi_{n,2}) = \\ & = -\beta_{n,1}\frac{d\varphi_{n,1}(t)}{dt} + M_0, \end{aligned} \tag{1}$$

$$\begin{aligned} & I_{n,2}\frac{d^2\varphi_{n,2}(t)}{dt^2} - K'_{n,2}\left[\varphi_{n+1,2}(t) - 2\varphi_{n,2}(t) + \varphi_{n-1,2}(t)\right] + \\ & + k_{n,1-2}R_{\mathrm{n},2}(R_{\mathrm{n},1} + R_{\mathrm{n},2})\sin\varphi_{n,2} - k_{\mathrm{n},1\text{-}2}R_{\mathrm{n},1}R_{\mathrm{n},2}\sin(\varphi_{n,2} - \varphi_{n,1}) = \\ & = -\beta_{n,2}\frac{d\varphi_{n,2}(t)}{dt} + M_0. \end{aligned} \tag{2}$$

Here, $\varphi_{1,n}(t)$ and $\varphi_{2,n}(t)$ are the angular displacements of nitrous bases in the main and complementary DNA chains, n is the number of the base pair, n = 1, 2, …N, N is the total number of base pairs, $I_{n,i}$ is the moment of inertia of the n-th nitrogenous base of the i-th chain, $R_{n,i}$ is the distance from the center of mass of the n-th nitrogenous base of the i-th chain to the sugar-phosphate backbone, $K'_{n,i}=KR^2_{n,i}$, K is the rigidity of the sugar-phosphate backbone, $\beta_{n,i}=\alpha R^2_{n,i}$, α is the dissipation coefficient, $k_{n,i}$ is a constant characterizing the interaction between bases within pairs, i = 1, 2, and M_0 is a constant torsion moment. 2N equations simulating the dynamics of the displacements have the form of coupled discrete sine-Gordon equations modified to take into account dissipation effects and the action of a constant torsion moment M_0 [14].

To solve the equations, Grinevich and coauthors applied the long-wave approximation. This made it possible to reduce the 2N discrete Equations 1 and 2 into two nonlinear partial differential

equations (NLPDEs). In general, several analytical schemes [19–24] exist to solve NLPDEs. However, here we use a different, simpler scheme. According to this scheme, let us take into account the distribution features of interactions within the DNA molecule: strong (covalent) interactions along the polynucleotide chains and weak interactions (hydrogen bonds) between polynucleotide chains. Then, model equations can be approximately reduced to two independent sine-Gordon equations

$$\bar{I}_1\varphi_{1,tt} - \bar{K}'_1 a^2\varphi_{1,zz} + \bar{k}_{1-2}\bar{R}_1^2 \sin\varphi_1 = -\bar{\beta}_1\varphi_{1.t} + M_0, \quad (3)$$

$$\bar{I}_2\varphi_{2.tt} - \bar{K}'_2 a^2\varphi_{2,.zz} + \bar{k}_{1-2}\bar{R}_2^2 \sin\varphi_1 = -\bar{\beta}_2\varphi_{2,t} + M_0, \quad (4)$$

having the kink-like solutions (or simply kinks):

$$\varphi_{k,1}(z,t) = 4\text{arctg}\{\exp[(\bar{\gamma}_1/\bar{d}_1)(z - \upsilon_{k,1}(t)\cdot t - z_{0,1})]\}. \quad (5)$$

$$\varphi_{k,2}(z,t) = 4\text{arctg}\{\exp[(\bar{\gamma}_2/\bar{d}_2)(z - \upsilon_{k,2}(t)\cdot t - z_{0,2})]\}. \quad (6)$$

Let us call solution (5) the first kink, and solution (6) the second kink. In formulas (5) and (6), $\upsilon_{k,1}(t)$ and $\upsilon_{k,2}(t)$ are the velocities of the first and second kinks; $\bar{\gamma}_1 = (1 - \upsilon_{k,1}^2/\bar{C}_1^2)^{-\frac{1}{2}}$ and $\bar{\gamma}_2 = (1 - \upsilon_{k,2}^2/\bar{C}_2^2)^{-\frac{1}{2}}$ are the Lorentz factors; $\bar{C}_1 = (\bar{K}'_1 a^2/\bar{I}_1)^{1/2}$ and $\bar{C}_2 = (\bar{K}'_2 a^2/\bar{I}_2)^{1/2}$ are the sound velocities; $z_{0,1}$ and $z_{0,2}$ are the coordinates of the first and second kinks at the initial moment of time; $\bar{I}_1$ is the moment of inertia of nitrogen bases of the first chain; $\bar{I}_2$ is the moment of inertia of nitrogen bases of the second chain; $\bar{K}'_1 = K\bar{R}_1^2$, $\bar{K}'_2 = K\bar{R}_2^2$, K is the rigidity of the sugar-phosphate backbone; $\bar{R}_1$ is the distance from the center of mass of the nitrogen bases of the first polynucleotide chain to the sugar-phosphate backbone; $\bar{R}_2$ is the distance from the center of mass of the nitrogenous bases of the second polynucleotide chain to the sugar-phosphate backbone; and a is the distance between the nearest pairs of bases. The dashes above the coefficients mean averaging over the length of the DNA fragment under consideration. The dynamic DNA parameters corresponding to different regions of the pPF1 plasmid are presented in Table 1.

Table 1. DNA dynamic parameters corresponding to different regions of the main and complementary sequences of the pPF1 plasmid [14].

Region of the main / complementary sequence	$\bar{I}_1\times10^{-44}$ / $\bar{I}_2\times10^{-44}$ (kg·m^2)	$\overline{K'}_1\times10^{-18}$ / $\overline{K'}_2\times10^{-18}$ (N·m)	$\bar{V}_1\times10^{-20}$ / $\bar{V}_2\times10^{-20}$ (J)
1+7	6.21 / 6.18	1.94 / 1.94	2.23 / 2.23
2 (*Egfp*)	6.16 / 6.22	1.92 / 1.95	2.28 / 2.30
3	6.21 / 6.21	1.96 / 1.96	2.04 / 2.04
4 (*mCherry*)	6.30 / 6.08	1.96 / 1.90	2.32 / 2.27
5	6.06 / 6.33	1.91 / 1.98	2.14 / 2.21
6 (*Kan*)	6.18 / 6.22	1.95 /1.95	2.13 / 2.14

In the framework of the model, the energy and size of the first and second kinks are determined by the following formulas:

$$\overline{E}_{k,1}(t) = \frac{\overline{E}_{01}}{\sqrt{1-(v_{k,1}(t)/\overline{C}_1)^2}}, \tag{7}$$

$$\overline{E}_{k,2}(t) = \frac{\overline{E}_{02}}{\sqrt{1-(v_{k,2}(t)/\overline{C}_2)^2}}, \tag{8}$$

$$\overline{D}_{k.1}(t) = \overline{d}_1\sqrt{1-(v_{k,1}(t)/\overline{C}_1)^2}, \tag{9}$$

$$\overline{D}_{k.2}(t) = \overline{d}_2\sqrt{1-(v_{k,2}(t)/\overline{C}_2)^2}, \tag{10}$$

where $\overline{E}_{01} = 8\sqrt{\overline{K}_1'\overline{V}_1}$ and $\overline{E}_{02} = 8\sqrt{\overline{K}_2'\overline{V}_2}$ are the rest energies of the first and second kinks; $\overline{d}_1 = (\overline{K}_1' a^2/\overline{V}_1)^{1/2}$ and $\overline{d}_2 = (\overline{K}_2' a^2/\overline{V}_2)^{1/2}$ are the sizes of the first and second kinks at rest; $\overline{V}_1 = \overline{k}_{1-2}\overline{R}_1^2$, $\overline{V}_2 = \overline{k}_{1-2}\overline{R}_2^2$; $\overline{k}_{1-2}$ is a constant that characterizes the interaction between bases within pairs.

The velocities of the first and second kinks, found in [15] using the McLaughlin-Scott method [25], have the form:

$$v_{k,1}(t) = \frac{\left[\left(v_{0,1}\overline{\gamma}_{0,1} - \frac{\overline{C}_1 M_0 \pi}{4\overline{\beta}_1}\sqrt{\frac{\overline{I}_1}{\overline{V}_1}}\right)\exp\left(-\frac{\overline{\beta}_1}{\overline{I}_1}(t-t_0)\right) + \frac{\overline{C}_1 M_0 \pi}{4\overline{\beta}_1}\sqrt{\frac{\overline{I}_1}{\overline{V}_1}}\right]}{\sqrt{1+\left[\left(\frac{v_{0,1}}{\overline{C}_1}\overline{\gamma}_{0,1} - \frac{M_0\pi}{4\overline{\beta}_1}\sqrt{\frac{\overline{I}_1}{\overline{V}_1}}\right)\exp\left(-\frac{\overline{\beta}_1}{\overline{I}_1}(t-t_0)\right) + \frac{M_0\pi}{4\overline{\beta}_1}\sqrt{\frac{\overline{I}_1}{\overline{V}_1}}\right]^2}}. \tag{11}$$

$$v_{k,2}(t) = \frac{\left[\left(v_{0,2}\overline{\gamma}_{0,2} - \frac{\overline{C}_2 M_0 \pi}{4\overline{\beta}_2}\sqrt{\frac{\overline{I}_2}{\overline{V}_2}}\right)\exp\left(-\frac{\overline{\beta}_2}{\overline{I}_2}(t-t_0)\right) + \frac{\overline{C}_2 M_0 \pi}{4\overline{\beta}_2}\sqrt{\frac{\overline{I}_2}{\overline{V}_2}}\right]}{\sqrt{1+\left[\left(\frac{v_{0,2}}{\overline{C}_2}\overline{\gamma}_{0,2} - \frac{M_0\pi}{4\overline{\beta}_2}\sqrt{\frac{\overline{I}_2}{\overline{V}_2}}\right)\exp\left(-\frac{\overline{\beta}_2}{\overline{I}_2}(t-t_0)\right) + \frac{M_0\pi}{4\overline{\beta}_2}\sqrt{\frac{\overline{I}_2}{\overline{V}_2}}\right]^2}}. \tag{12}$$

Here, $v_{0,1}$, $v_{0,2}$ are the initial velocities of the first and second kinks, respectively; $\overline{\gamma}_{0,1} = (1 - v_{0,1}^2/\overline{C}_1^2)^{-\frac{1}{2}}$, $\overline{\gamma}_{0,2} = (1 - v_{0,2}^2/\overline{C}_2^2)^{-\frac{1}{2}}$; M_0 is the torsion moment.

2.1. Energetics of the first kink

The energy profile is an important characteristic of kink energetics, reflecting the features of the potential field where the kink moves. Figure 2 shows the result of energy profile calculations made for the case of the first kink using formula (7) and the data from Table 1. The obtained numerical estimations of the rest energy of the first kink in different regions of the pPF1 plasmid are presented in Table 2. This table also presents estimations of the size of the first kink at rest in various regions of the pPF1 plasmid. To obtain these results, Equation (9) was used.

Table 2. Rest energy and size of the first kink.

Regions	$\overline{E}_{01}\times10^{-18}$ (J)	$\overline{d}_1\times10^{-9}$ (m)
1+7	1.67	3.17
2 (*Egfp*)	1.67	3.12
3	1.60	3.33
4 (*mCherry*)	1.71	3.13
5	1.62	3.23
6 (*Kan*)	1.63	3.25

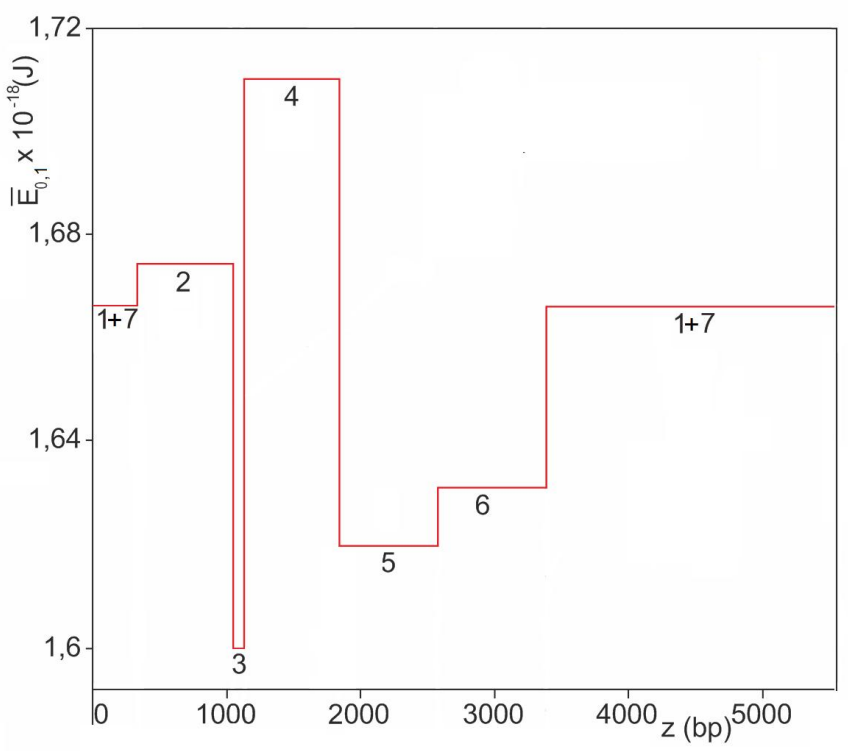

Figure 2. Energy profile of the potential field in which the first kink moves.

From Figure 2, it can be seen that the deepest well in the energy profile is located in the third region. This means that the formation of the kink in this region requires the least energy expenditure. In subsequent calculations, we use this result, assuming that at the initial moment of time, the first kink is activated in the center of the third region ($z_{0,1} = 1092$ bp, 1 bp =3.4×10^{-10} m) with the initial velocity $v_{0,1} = 0$ and the rest energy $\overline{E}_{01} = 1.60 \times 10^{-18}$ J.

In Figures 3a and 3d, we present the time dependence of the first kink energy, obtained using Equations (7) and (11). For comparison, the time dependence of the size and velocity of the first kink is also provided (Figure 3b, 3c, 3e, and 3f). The graphs presented in Figure 3 on the left were obtained for the model value of the torsion moment $M_0 = 2.50 \times 10^{-22}$ J. The results shown in Figure 3 on the right were obtained for the model value of the torsion moment $M_0 = 6.50 \times 10^{-22}$ J.

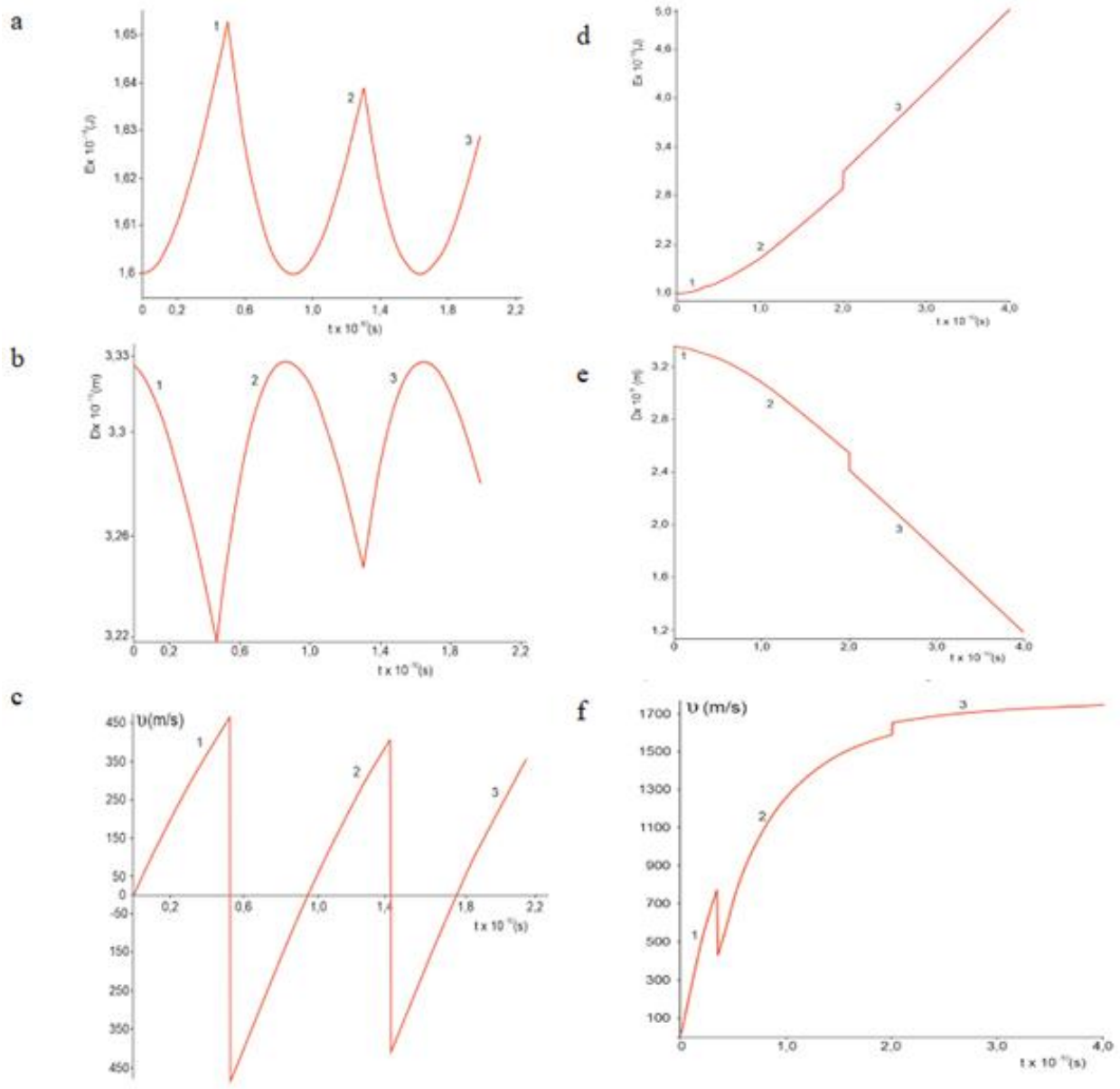

Figure 3. Time dependences of the energy (a, d), size (b, e), and velocity (c, f) of the first kink. The results obtained for the case of $M_0 = 2.50 \times 10^{-22}$ J are shown on the left, and for the case of $M_0 = 6.50 \times 10^{-22}$ J on the right.

2.1.1. The case $M_0 = 2.50 \times 10^{-22}$ J

It is evident from Figure 3a that in the first time interval (0; 5.45×10^{-11} s), which is determined by the time from the start of the kink movement until the moment it reaches the right boundary of the third region, the kink energy increases from 1.60×10^{-18} J to 1.65×10^{-18} J (curve 1). The kink size (Figure 3b, curve 1) smoothly decreases from 3.33×10^{-9} m to 3.22×10^{-9} m, and the kink velocity (Figure 3c, curve 1) smoothly increases from zero to the maximum value of 476.73 m/s.

At the moment of time 5.45×10^{-11} s, the kink, having reached the right boundary, changes the

movement to the opposite direction, which corresponds to a sharp vertical drop of curve 1 in Figure 3c from 476.73 m/s to –476.73 m/s.

In the second time interval (5.45×10^{-11}; 1.42×10^{-10} s), the kink energy first smoothly decreases from 1.65×10^{-18} J to 1.60×10^{-18} J, and then smoothly increases to 1.64×10^{-18} J (Figure 3a, curve 2). The kink size in this time interval, on the contrary, first increases from 3.22×10^{-9} m to 3.33×10^{-9} m, and then smoothly decreases to 3.25×10^{-9} m (Figure 3b, curve 2). The kink velocity smoothly increases from –476.73 m/s to 411.50 m/s (Figure 3c, curve 2).

At the end of the second time interval, the kink again reaches the right boundary of the third region, and then a new cycle of kink movement in the time interval 1.42×10^{-10}; 2.40×10^{-10} s begins. This cycle includes a change in the direction of the kink movement to the opposite, a smooth movement of the kink from the right boundary to the left boundary, a smooth turn by 180° before reaching the left boundary, and a smooth movement back to the right boundary, as well as a reflection from this boundary (curves 3 in Figures 3a, 3b, and 3c).

It is obvious that such cycles will be repeated in the following time intervals. In this case, the maximum values of the kink energy on the right boundary will decrease and, in the limit, will tend to the rest kink energy $E_{01} = 1.60 \times 10^{-18}$ J. The values of the kink size on the right boundary will increase and, in the limit, will tend to the size of the kink at rest $\bar{d}_1 = 3.33 \times 10^{-9}$ m. The values of the kink velocity on the right boundary will decrease and, in the limit, will tend to zero.

2.1.2. The case $M_0 = 6.50 \times 10^{-22}$ J

As follows from Figure 3 that the time dependence of the energy, size, and velocity for the case $M_0 = 6.50 \times 10^{-22}$ J differ significantly from those obtained in the case of $M_0 = 2.50 \times 10^{-22}$ J.

Indeed, in the first time interval (0; 3.42×10^{-11} s), as in the previous case, a smooth increase in the kink energy (Figure 3d, curve 1), a smooth decrease in the kink size (Figure 3e, curve 1), and a smooth increase the kink velocity (Figure 3f, curve 1) are observed.

However, in the second time interval (3.42×10^{-11}; 2.00×10^{-10} s), unlike the previous case, the kink energy continues to increase smoothly (Figure 3d, curve 2), the kink size continues to decrease smoothly (Figure 3e, curve 2), and the kink velocity continues to increase smoothly (Figure 3f, curve 2). This indicates that the first kink overcomes the right boundary of the third region to continue its movement in the neighboring fourth region.

In the next time interval (2.00×10^{-10}; 4.00×10^{-10} s), the kink energy continues to increase smoothly (Figure 3d, curve 3), the kink size continues to decrease smoothly (Figure 3e, curve 3), and the kink velocity continues to increase smoothly (Figure 3f, curve 3). This indicates that the first kink overcomes the right boundary of the fourth region and continues moving in the fifth region. Thus, there are no oscillatory features in the energy and dynamic behavior of the kink. On the contrary, both dynamic and energy characteristics change smoothly (gradually increasing or decreasing). Small zigzags at the boundaries of time intervals are explained by our assumption about the nonradiative nature of crossing these boundaries.

Comparing the results presented on the left and right in Figure 3, we conclude that there is a threshold value of the torsion moment $M_{0,\text{crit}}$ below which the kink energy is oscillatory in nature and above which it is translational. A similar conclusion, but only regarding the dynamic properties of the pPF1 plasmid, was made in [15]. The threshold value of the torsion moment $M_{0,\text{crit}}$ estimated in this work was $M_{0,\text{crit}} = 4.95 \times 10^{-22}$ J.

2.2. Energetics of the second kink

To obtain the energy profile that determines the features of the second kink movement in the pPF1 plasmid (Figure 4), we used Equation (4) and data from Table 1. The results of the rest energy and the size of the second kink in different regions of the pPF1 plasmid are presented in Table 3.

Table 3. Rest energy and size of the second kink.

Regions	$\overline{E}_{02}10^{-18}$ (J)	$\overline{d}_2\times10^{-9}$ (m)
1+7	1.66	3.17
2 (*Egfp*)	1.69	3.14
3	1.60	3.33
4 (*mCherry*)	1.66	3.11
5	1.67	3.22
6 (*Kan*)	1.63	3.24

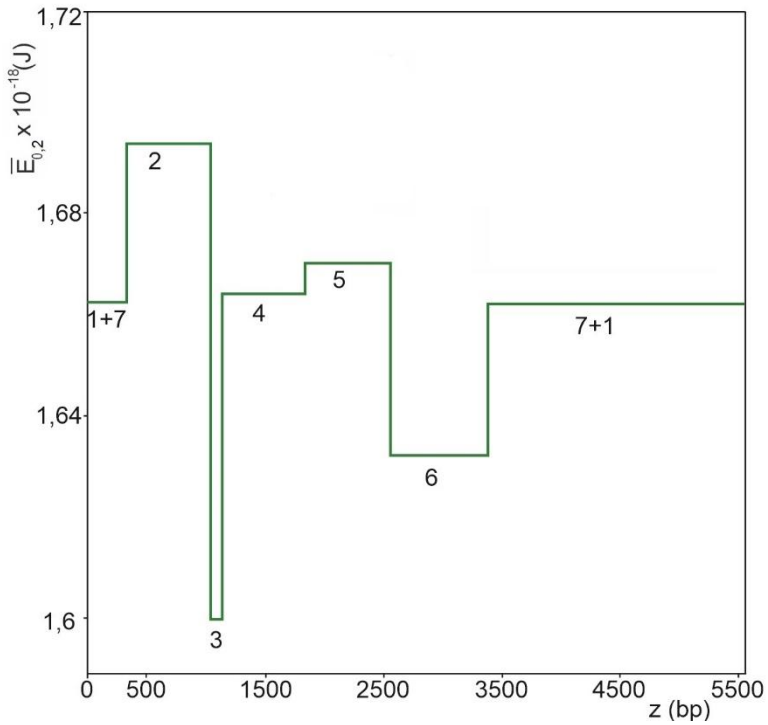

Figure 4. Energy profile of the potential field in which the second kink moves.

It is evident from Figure 4 that the deepest well in the energy profile is located in the third region. Therefore, in our calculations for the case of the second kink, we also assume that at the initial moment of time, the kink is activated in the center of the third region ($z_{0,1}$ = 1092 bp, 1 bp = 3.4×10^{-10} m) with the initial velocity $v_{0,1} = 0$ and rest energy $\overline{E}_{02} = 1.60 \times 10^{-18}$ J.

Using Equations (4) and (8), we constructed graphs of the time dependence of the energy of the second kink (Figure 5), moving under the action of a constant torsion moment M_0 from right to left; also, we provided graphs of the time dependence of the size and velocity of the second kink for

comparison. The results were obtained for two model values of the torsion moment: $M_0 = -2.50 \times 10^{-22}$ J and $M_0 = -6.50 \times 10^{-22}$ J.

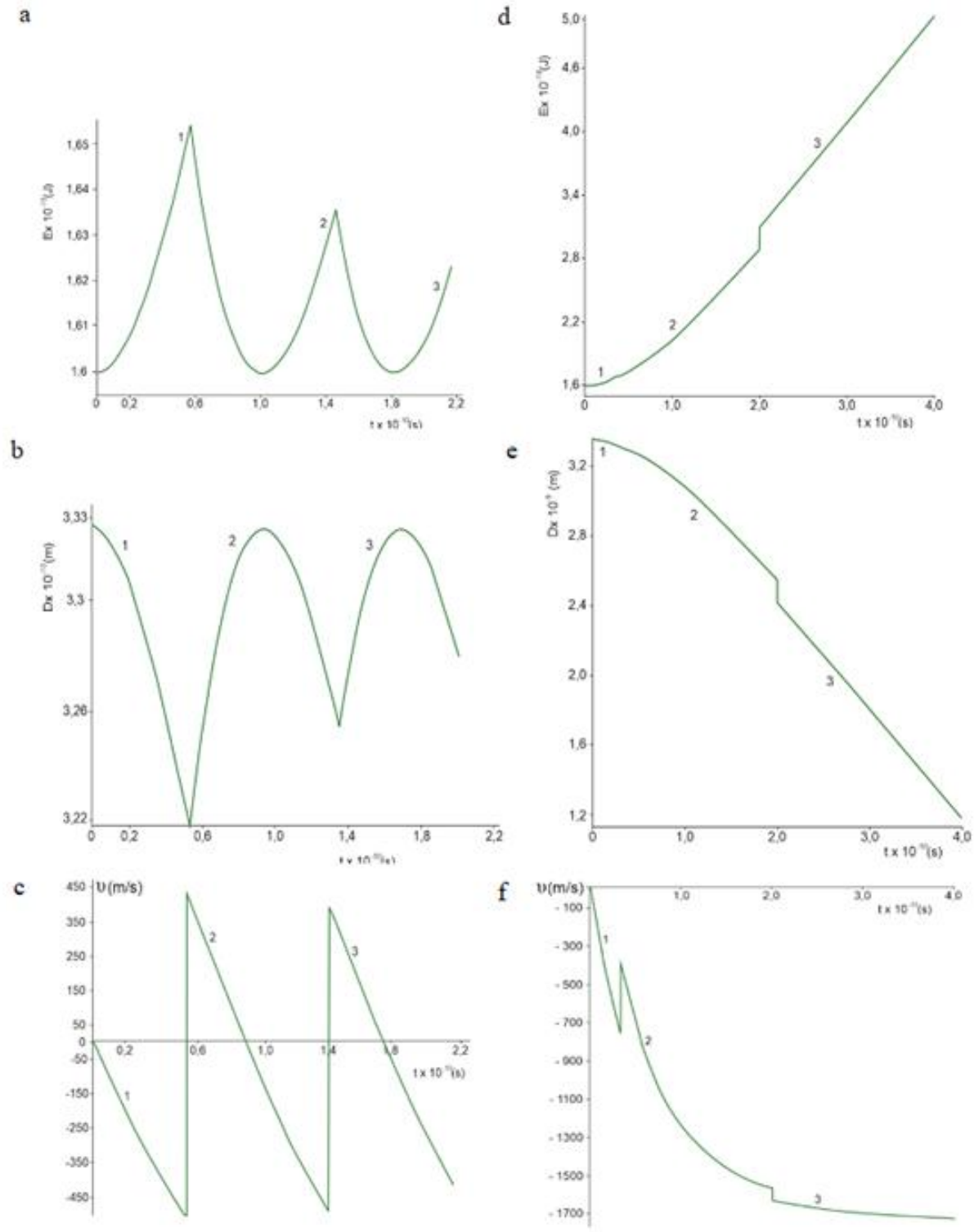

Figure 5. Time dependence of the energy (a, d), size (b, e), and velocity (c, f) of the second kink. The results obtained for the case of $M_0 = -2.50 \times 10^{-22}$ J are shown on the left and for the case of $M_0 = -6.50 \times 10^{-22}$ J on the right.

2.2.1. The case $M_0 = -2.50 \times 10^{-22}$ J

From the graphs presented in Figure 5 on the left, it is evident that in the first time interval (0; 5.55×10^{-11} s), which is determined by the time it takes for the second kink to reach the left boundary of the third region, kink energy increases from 1.60×10^{-18} J to 1.65×10^{-18} J (Figure 5a, curve 1). The kink size (Figure 5b, curve 1) smoothly decreases from 3.33×10^{-9} m to 3.22×10^{-9} m, and the kink velocity (Figure 5c, curve 1) smoothly decreases from zero to −479.00 m/s.

At the moment of time 5.55×10^{-11} s, the second kink is reflected from the left boundary of the third region, and its velocity changes direction to the opposite, which corresponds to a sharp vertical rise of curve 1 in Figure 5c from −479.00 m/s to 479.00 m/s.

In the second time interval (5.55×10^{-11}s; 1.41×10^{-10} s), the kink energy first smoothly decreases from 1.65×10^{-18} J to 1.60×10^{-18} J and then smoothly increases to 1.63×10^{-18} J (Figure 5a, curve 2). The kink size in this time interval (Figure 5b, curve 2), on the contrary, first increases from 3.22×10^{-9} m to 3.33×10^{-9} m, and then smoothly decreases to 3.25×10^{-9} m. The kink velocity in this case smoothly decreases from 411.32 m/s to −479.00 m/s (Figure 5c, curve 2).

At the end of the second time interval, at the moment of time 1.41×10^{-10} s, the second kink again appears on the left boundary of the third region, and then a new cycle of the kink movement in the time interval 1.41×10^{-10} s; 2.40×10^{-10} s begins. This cycle includes a change in kink movement to the opposite direction, a smooth movement of the kink from the left boundary in the direction of the right boundary, a smooth turn by 180° before reaching the right boundary, and a smooth movement back to the left boundary, as well as a reflection from this boundary (Figure 5c, curve 3).

In the following time intervals, such cycles will be repeated. The maximum values of kink energy on the left boundary of the third section will decrease and, in the limit, tend to the kink rest energy $\overline{E}_{02} = 1.60 \times 10^{-18}$ J. The values of the kink size on the left boundary will increase and, in the limit, will tend to $\overline{d}_1 = 3.33 \times 10^{-9}$ m; the values of the kink velocity on the left boundary will decrease and, in the limit, will tend to zero.

2.2.2. The case $M_0 = -6.50 \times 10^{-22}$ J

From the graphs presented in Figure 5 on the right, it is clear that the energetics of the second kink for the case of $M_0 = -6.50 \times 10^{-22}$ J differ significantly from the previous case.

Indeed, in the first time interval (0; 3.40×10^{-11} s), a smooth increase in kink energy is observed (Figure 5d, curve 1). In the same time interval, the kink size smoothly decreases (Figure 5d, curve 1), and the velocity also smoothly decreases (Figure 5e, curve 1).

In the next time interval (3.40×10^{-11}; 2.00×10^{-10} s), kink energy continues to increase smoothly (Figure 5d, curve 2), kink size continues to decrease (Figure 5e, curve 2), and kink velocity also continues to decrease (Figure 5f, curve 2). This indicates that the kink has overcome the left boundary of the third region and continued its smooth translational motion in the neighboring second region. The small zigzags in Figures 5e and 5f are the result of using an approximation that assumes a nonradiative transition across the boundary.

In the third time interval (2.00×10^{-10} s; 4.00×10^{-10} s), kink energy continues to increase smoothly (Figure 5d, curve 3), kink size continues to decrease (Figure 5e, curve 3), and kink velocity continues to decrease (Figure 5f, curve 3). This indicates that the second kink overcomes the left boundary of the second region and continues its smooth translational motion in the adjacent (1+7)th region.

Thus, the dynamics and energy of the kink do not exhibit any oscillatory character at all. On the contrary, both the dynamic and energy characteristics change smoothly and gradually, with the exception of small zigzags at the boundaries of time intervals, which are explained by our assumption about the nonradiative nature of crossing these boundaries.

Comparing the graphs presented on the left and right sides of Figure 5, we conclude that there is a threshold value of the torsion moment $M_{0,\mathrm{crit}}$, below which kink energy is oscillatory in nature, and above which it is translational. The estimate of $M_{0,\mathrm{crit}}$ obtained in [15] from the analysis of kink dynamics gives a value equal to $M_{0,\mathrm{crit}} = -4.20 \times 10^{-22}$ J.

3. Conclusion

In this work, the energetics of kinks formed and moving in the pPF1 plasmid were investigated. The model of Grinevich and coauthors was used to mathematically describe kink movement. Within the framework of the model, the plasmid sequence was divided into several regions, including the Egfp, mCherry, and Kan genes, as well as intermediate regions between them, and the coefficients of the model equations were averaged over each of these regions.

It was shown that activation of two types of kinks was possible in the pPF1 plasmid. These two types of kinks were considered as two types of quasiparticles having their own energy, mass, and velocity, and moving in the potential field of the plasmid. The profiles of the potential field were calculated. It was found that the lowest energy required for both types of kink formation was observed in the third region of the plasmid sequence located between the genes for the red (*mCherry*) and green (*Egfp*) proteins.

The time dependence of the energy and size of kinks propagating along the main and complementary sequences of the pPF1 plasmid was calculated. The form of the curves of time dependence was completely determined by the magnitude of the torsion moment M_0. In particular, when the torsion moment values were lower than the threshold values ($M_{0,\mathrm{crit,1kink}} = 4.95 \times 10^{-22}$ J for the first kink and $M_{0,\mathrm{crit,2kink}} = 4.20 \times 10^{-22}$ J for the second kink), the curves reflecting the time changes in energy had the form of damped oscillations. When the torsion moment values were greater than the threshold values, the energy curves smoothly increased.

However, all the above results were obtained within the framework of a model that included a number of simplifications and limitations. The model took into account angular oscillations of nitrogenous bases and did not consider longitudinal and transverse displacements of nucleotides, which are also important. The model also did not consider the effects associated with kinks crossing boundaries. When performing calculations, instead of exact methods, approximate ones were used, namely a quasi-homogeneous approximation, the block method, and the McLaughlin-Scott method.

Despite these shortcomings, the simplicity and convenience of the approach described above make it very attractive. This approach can be successfully used to study the behavior of kinks not only in plasmids but also in any other DNA molecules. It can also be noted that the mathematical apparatus used here can find wider applications, for example, in the physics of inhomogeneous crystals, Earth physics, nonlinear optics, and others where the sine-Gordon equation and its modifications are used.

Use of AI tools declaration

The authors declare they have not used Artificial Intelligence (AI) tools in the creation of this article.

Conflict of interest

All authors declare no conflicts of interest in this paper.

References

1. Zdravković S (2022) Nonlinear dynamics of DNA chain, In: Zdravković S, Chevizovich D, *Nonlinear Dynamics of Nanobiophysics,* Singapore, Springer: 29–66. https://doi.org/10.1007/978-981-19-5323-1_3
2. Zoli M (2022) Non-linear Hamiltonian models for DNA. *Eur Biophys J* 51: 431–447. https://doi.org/10.1007/s00249-022-01614-z
3. Englander W, Kallenbach NR, Heeger AJ, et al. (1980) Nature of the open state in long polynucleotide double helices: possibility of soliton excitations. *Proc Natl Acad Sci USA* 77: 7222–7226. https://doi.org/10.1073/pnas.77.12.7222
4. Yomosa S (1983) Soliton excitations in deoxyribonucleic acid (DNA) double helices. *Phys Rev A* 27: 2120–2125. https://doi.org/10.1103/PhysRevA.27.2120
5. Takeno S, Homma S (1983) Topological solitons and modulated structure of bases in DNA double helices. *Prog Theor Phys* 70: 308–311. https://doi.org/10.1143/PTP.70.308
6. Krumhansl JA, Alexander DM (1983) Nonlinear dynamics and conformational excitations in biomolecular materials, In: Clementi E, Sarma RH, Structure and dynamics: nucleic acids and proteins, New York: Adenine Press, 61–80.
7. Fedyanin VK, Gochev I, Lisy V (1986) Nonlinear dynamics of bases in continual model of DNA double helices. *Stud Biophys* 116: 59–64.
8. Yakushevich LV (1989) Nonlinear DNA dynamics: a new model. *Phys Lett A* 136: 413–417.
9. Grinevich AA, Yakushevich LV (2018) The influence of the DNA torque on the dynamics of transcription bubbles in plasmid PTTQ18. *J Theor Biol* 453: 68–77. https://doi.org/10.1016/j.jtbi.2018.04.036
10. Masulis IS, Babaeva ZS, Chernyshov SV, et al. (2015) Visualizing the activity of Escherichia coli divergent promoters and probing their dependence on superhelical density using dual-colour fluorescent reporter vector. *Sci Rep* 5: 11449. https://doi.org/10.1038/srep11449
11. Shavkunov KS, Masulis IS, Tutukina MN, et.al (2009) Gains and unexpected lessons from genome-scale promoter mapping *Nucleic Acids Res* 37: 4919–4931. https://doi.org/10.1093/nar/gkp490
12. Masulis IS, Grinevich AA, Yakushevich LV (2024) Dynamics of open states and promoter functioning in the appY_red and appY_green genetic constructions based on the pPF1 plasmid. *Front Biosci-Landmark* 29: 155. https://doi.org/10.31083/j.fbl2904155

13. Grinevich AA, Masulis IS, Yakushevich LV (2021) Mathematical modeling of transcription bubble behavior in the pPF1 plasmid and its modified versions: the link between the plasmid energy profile and the direction of transcription. *Biophysics* 66: 209–217. https://doi.org/10.1134/S000635092102007X
14. Krasnobaeva LA, Yakushevich LV (2022) DNA kinks behavior in the potential pit-trap. *AIMS Biophys* 9: 130–146. https://doi.org/10.3934/biophy.2022012
15. Krasnobaeva LA, Yakushevich LV (2024) Trajectories of solitons movement in the potential field of pPF1 plasmid with non-zero initial velocity. *Math Model* 19: 232–247. https://doi.org/10.17537/2024.19.232
16. The red protein mCherry sequence and map. Available from: https://www.fpbase.org/protein/mcherry/.
17. The green protein Egfp sequence and map. Available from: https://www.fpbase.org/protein/egfp/.
18. The kanamycin sequence and map. Available from: https:// go.drugbank.com›drugs/DB01172/.
19. Cao Y, Malomed BA, He J (2018) Two (2+1)-dimensional integrable nonlocal nonlinear Schrödinger equations: breather, rational and semi-rational solutions. *Chaos Solitons Fractals* 114: 99–107. https://doi.org/10.1016/j.chaos.2018.06.029
20. Bhatti MM, Lu DQ (2019) Hydroelastic solitary wave during the head-on collision process in a stratified fluid. *Proc Inst Mech Eng Part C* 233: 6135–6148. https://doi.org/10.1177/0954406219861135
21. Younas U, Younis M, Seadawy AR, et al. (2021) Diverse exact solutions for modified nonlinear Schrödinger equation with conformable fractional derivative. *Results Phys* 20: 103766. https://doi.org/10.1016/j.rinp.2020.103766
22. Eslami M (2016) Trial solution technique to chiral nonlinear Schrödinger's equation in (1+2)-dimensions. *Nonlinear Dyn* 85: 813–816. https://doi.org/10.1007/s11071-016-2724-2
23. Aslan I (2014) Exact solutions of a fractional-type differential-difference equation re- lated to discrete MKdv equation. *Commun Theor Phys* 61: 595. https://doi.org/10.1088/0253-6102/61/5/09
24. El-Rashidy K, Seadawy AR, Althobaiti S, et al. (2020) Multiwave kinky breathers and multi-peak soliton solutions for the nonlinear Hirota dynamical system. *Results Phys* 19: 103678. https://doi.org/10.1016/j.rinp.2020.103678
25. McLaughlin DW, Scott AC (1978) Perturbation analysis of fluxon dynamics. *Phys Rev A* 18: 1652. https://doi.org/10.1103/PhysRevA.18.1652